

# HARNESSING ENZYMATICALLY MACHINED NANO- AND MICRO-SCALE SURFACE TOPOGRAPHIES FOR HIGH-THROUGHPUT SEPARATIONS

Jen-Huang Huang, Aashish Priye, Arul Jayaraman, Victor M. Ugaz

Department of Chemical Engineering  
Texas A&M University, College Station, TX, USA

## ABSTRACT

We show how enzymatic activity can be harnessed as a tool to fashion complex nano- and micro-scale surface topographies on biodegradable substrates. Coordinated patterning and machining are accomplished by manipulating interactions between an enzyme, substrate, and protein inhibitor. In this way, we are able to construct nanochannels, microchannels containing embedded features templated by the substrate's crystalline morphology, and a membraneless filter capable of isolating rare cells from whole blood with throughput orders of magnitude greater than currently possible. In addition to enabling molecularly imprinted surface landscapes mimicking those in living systems to be fashioned via a straightforward process accessible in virtually any laboratory, considerable potential exists to exquisitely control the underlying biochemical interactions by employing enzymes and substrates with appropriately engineered properties.

## KEYWORDS

Separations, inertial microfluidics, microfabrication, nanofabrication, cell separations.

## INTRODUCTION

We have developed a microfabrication approach that harnesses biochemical interactions between an enzyme and a biodegradable substrate to enable localized and precisely controlled etching (Fig. 1). This bio-sculpting process exploits the enzymatic activity of proteinase K (PK). Etching is initiated when PK is transported from bulk solution to the surface of a poly(lactic acid) (PLA) substrate, after which enzyme-substrate complexation catalyzes surface reactions yielding low molecular weight cleavage products that subsequently become hydrolyzed and are released back into the bulk along with dissociated PK (Fig. 1a). When an aqueous solution of PK is directed through a microchannel template, the ensuing enzymatic degradation imprints a replica of the flow path into a PLA substrate comprising the channel floor (Fig. 1b). Characteristic etching rates of 1–10  $\mu\text{m}/\text{h}$  are achievable. These rates enable nanometer-size features to be easily imprinted, as illustrated by construction of a 170 nm deep channel via injection of a PK solution at 2  $\mu\text{L min}^{-1}$  for 3 h at room temperature (Fig. 1c).

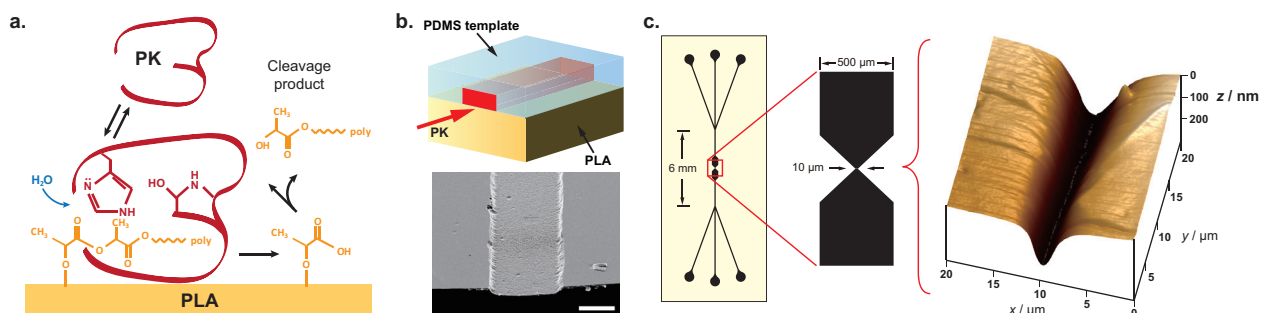


Figure 1. (a) Biochemical degradation cycle between proteinase K (PK) and the PLA substrate. (b) Cross-sectional schematic (above) illustrating how machining is performed by directing an aqueous PK solution through a PDMS microchannel template bonded to a PLA sheet (bar in SEM image below, 200  $\mu\text{m}$ ). (c) A nanochannel (170 nm deep) is constructed by injecting PK into a PDMS template (left) for 3 h at 25  $^{\circ}\text{C}$ . Machining is laterally confined within a  $\sim 4 \mu\text{m}$ -wide zone by hydrodynamic focusing of PK between co-injected streams of bovine serum albumin (2  $\mu\text{L min}^{-1}$  each stream). The z-axis of the AFM profile (right) is expanded to show detail.

## EXPERIMENT

Smooth planar substrates were obtained by placing pelletized PLA resin (NatureWorks, grade 3051D; Jamplast Inc.) directly onto glass microscope slides. A microfluidic etching template was prepared in poly(dimethyl siloxane) (PDMS) using soft lithography and directly adhered to the flat surface of a PLA substrate to produce enclosed channel networks. Aqueous solutions of proteinase K (MW = 28.9 kDa; Fisher Scientific) and bovine serum albumin (BSA; MW = 66.4 kDa) were prepared in 30 mM Tris-HCl buffer (pH 8.0, BP1758; Fisher Scientific). An etchant concentration of  $[\text{PK}] = 6.92 \mu\text{M}$  (0.2  $\text{mg mL}^{-1}$ ) was used in most experiments. A syringe pump (PHD 2000; Harvard Apparatus) was connected, and the entire assembly was placed inside an incubator while the etching solutions (enzyme, BSA, buffer) were continuously pumped through the network at 37  $^{\circ}\text{C}$ . Enclosed microchannels were constructed by thermally bonding the etched PLA replica to a flat PLA substrate at 80  $^{\circ}\text{C}$  for 20 min.

Complex cross-sectional topologies can be fashioned by establishing concentration gradients that spatially regulate the machining process. Feature definition is enhanced by replacing the buffer stream with a bovine serum albumin (BSA) solution to establish a competitive interaction that inactivates the laterally diffusing enzyme before it can attack the PLA. Microchannels where feature depths vary along the cross-section can be fashioned by sequentially changing composition and flow conditions (Fig. 2). The machined structures can be used as-is, or the rigid PLA can act as a re-usable mold for mass replication in PDMS.

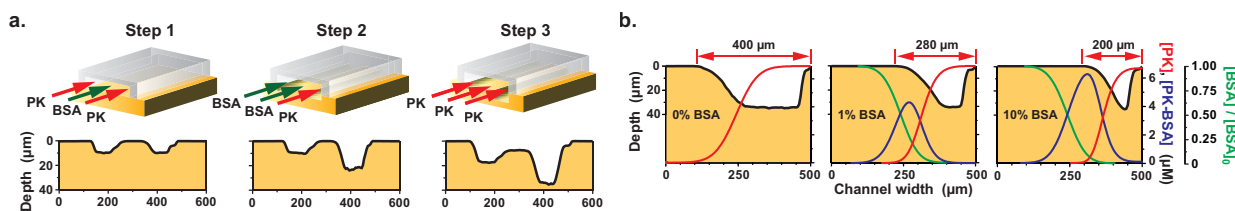


Figure 2. Machining is governed by a competitive interaction between enzyme, substrate, and inhibitor. (a) Alternating flows of PK and BSA are sequentially introduced to create microchannel profile where the depth varies along the cross-section. (b) Profilometry measurements of machined profiles 1 cm downstream from the inlet (black line; left ordinate) as a function of BSA concentration are overlaid with predicted lateral concentration profiles of free PK and PK-BSA complex (red and blue lines, respectively; inner right ordinate) and BSA normalized to the injected concentration (green line; outer right ordinate). Machining conditions:  $[PK] = 6.92 \mu\text{M}$  in the bulk solution,  $5 \mu\text{L}/\text{min}$ ,  $37^\circ\text{C}$ ,  $16 \text{ h}$ ,  $[BSA]_0 = 0.15$  and  $1.5 \text{ mM}$  for 1 and 10 % solutions, respectively.

## RESULTS AND DISCUSSION

We applied enzymatic machining to construct a new filtration architecture that uniquely overcomes the key limitations of previous methods investigated for size-based separations of blood cells. Our microfluidic design incorporates an embedded weir-like barrier oriented parallel to the flow direction and extending along the entire centerline length of a microchannel (Fig. 3a). This arrangement, combined with the transverse centrifugal flow generated within the microchannel's curved path, creates a driving force that transports smaller-sized components across the barrier from the inner lane to the outer lane while larger-sized species are retained in the inner lane.

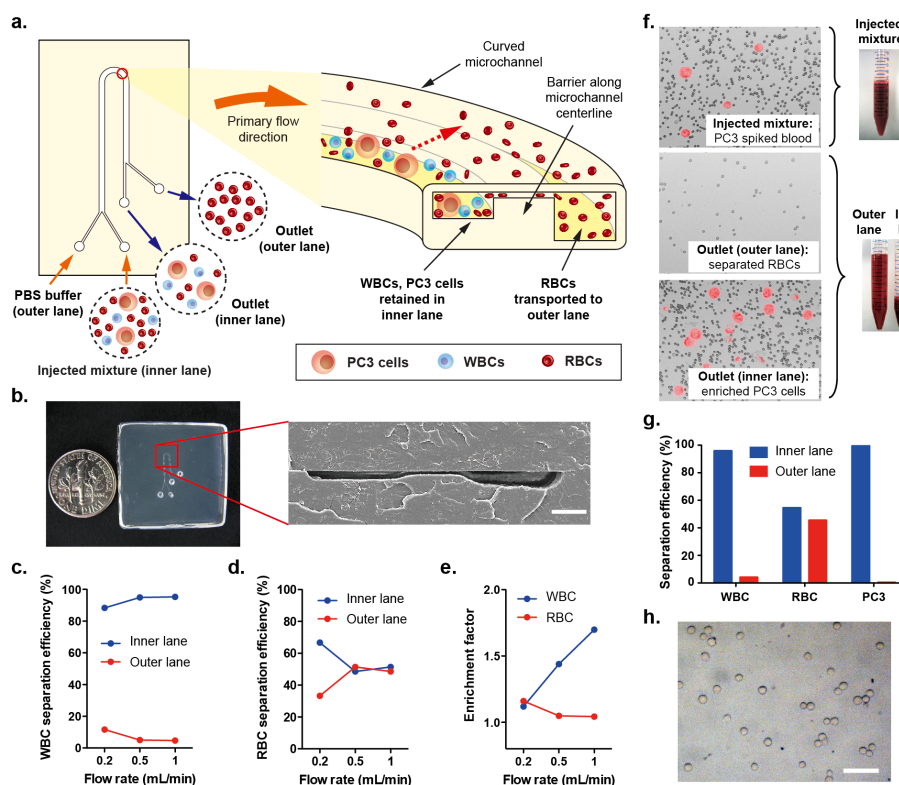


Figure 3. (a) Filtration architecture with embedded centerline barrier (inner and outer lanes:  $20$  and  $35 \mu\text{m}$  deep, centerline barrier gap:  $3 \mu\text{m}$  deep, radius of curvature:  $500 \mu\text{m}$ ). (b) Assembled device (left) and SEM of microchannel cross-section (right; bar,  $50 \mu\text{m}$ ). (c–e) Whole blood separation data. Cell counts reveal how relative fractions of (c) WBCs and (d) RBCs collected at the inner and outer lanes depend on flow rate. (e) Ratio of cell density collected at the inner lane relative to that in the injected mixture shows that WBC enrichment increases with flow rate (upper limit of  $1 \text{ mL}/\text{min}$  was imposed by our syringe pump). (f–h) Separation of whole blood spiked with PC3 cancer cells at  $1 \text{ mL}/\text{min}$ . (f) Isolation and enrichment of PC3 cells at inner lane. (g) Cell counts show relative fractions of WBCs, RBCs, and PC3 cells recovered at inner lane. (h) PC3 viability is unchanged after filtration.

Unequal depths on each side of the weir enable further enrichment of the separated species (Fig. 3b). Exploiting curvature-induced forces allows the filtration barrier to be oriented parallel to the flow direction rather than perpendicular to it, minimizing the pressure drop and avoiding clogging. Separation occurs most efficiently at high flow rates because the magnitude of the curvature-induced transverse flow is maximized, making our approach ideally suited for high-throughput analysis.

We first explored separation of red and white blood cells from whole blood to evaluate the effect of the applied flow rate. Whole blood was injected into the inner lane, and phosphate buffered saline (PBS) was co-injected into the outer lane at the same flow rate. Blood samples were diluted 1:5 with phosphate buffered saline (PBS) to minimize the viscosity mismatch between the inner and outer streams, enhancing separation efficiency by maximizing the transverse flow magnitude. Coulter counter analysis of the collected effluent reveals that 95% of the WBCs remain confined in the inner lane (Fig. 3c), whereas approximately half of the RBCs are transported across the barrier above a flow rate of 0.5 mL/min (Fig. 3d). WBC density in the inner lane increases with flow rate, while the RBC density remains relatively constant (Fig. 3e). Results are in agreement with hemacytometer-based counts.

To demonstrate practical application of this method, we used it to separate PC3 human prostate cancer cells (20 – 30  $\mu\text{m}$  diameter) from whole blood (Fig. 3f, injected component densities were PC3:  $1.43 \times 10^6$  cells/mL, WBC:  $1.22 \times 10^6$  cells/mL, RBC:  $7.32 \times 10^8$  cells/mL). The PC3 spiked blood sample was injected into the inner lane at 1 mL/min (PBS was co-injected into the outer lane at the same flow rate). Cell counts indicate that PC3 cells were separated with > 99% efficiency (Fig. 3g) with 1.6x enrichment upon recovery from the inner lane owing to the unequal depths on each side of the centerline barrier (45% of RBCs, 4 % of WBCs, and < 1 % of PC3 cells cross the centerline barrier to the outer lane). The enriched cells were maintained in the as-injected blood environment with no discernable change in viability (before filtration:  $98.7 \pm 0.6 \%$ ,  $n = 3$ ; after:  $98.9 \pm 0.1 \%$ ,  $n = 3$ ; Fig. 3h). Our method delivers  $99.2 \pm 0.2 \%$  ( $n = 3$ ) retention of PC3 cells from spiked whole blood and  $99.7 \pm 0.5 \%$  ( $n = 3$ ) when dispersed in PBS buffer. No additional steps are required to retrieve the separated cells, in contrast to conventional membrane or affinity capture.

The highly specific nature of enzyme-substrate interactions can also be exploited to enable direct imprinting of molecular-scale topologies. We explored this potential by taking advantage of the machining rate selectivity to PLA crystallinity to embed morphological features associated with the substrate's crystalline domains within a fluidic channel (Fig. 4a). The crystalline morphology is in turn governed by thermal history (annealing time and temperature, cooling rate) and material properties (molecular weight, stereoisomers and their blends), permitting broad control over the imprinted topologies. Machining after the PLA is continuously cooled from the melt exposes a dendritic surface topology, whereas an array of obstacles reflecting the size and density of spherulitic crystalline domains emerges when PK is injected following a low-temperature anneal (70  $^{\circ}\text{C}$  for 8 h) (Fig. 4b). By controlling annealing time and temperature, the extent and distribution of crystallinity within the substrate can be manipulated to enable post-like arrays with tunable size and density to be embedded within a micro- or nano-scale fluidic channel in a lithography-free manner (e.g., as barrier or packing structures for filtration and chromatography).

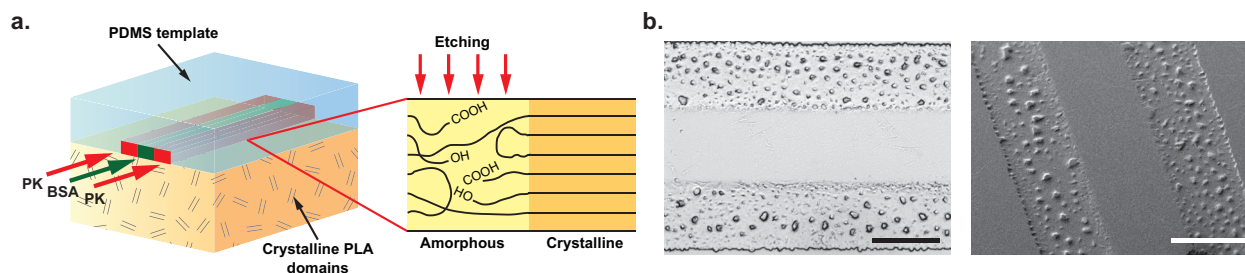


*Figure 4. (a) Morphologically governed selectivity is made possible by differences in the rate of PK-mediated degradation between hydrolysis-resistant crystalline domains and amorphous regions containing condensed hydrophilic and catalytic terminal groups ( $-\text{OH}$  and  $-\text{COOH}$ ). (b) Machining after annealing at 70  $^{\circ}\text{C}$  for 8 h embeds an array of post-like obstacles within the microchannel (a 3D topology is evident in the SEM image, right). PK was injected at 37  $^{\circ}\text{C}$  for 2 h (bars, 100  $\mu\text{m}$ ).*

In conclusion, enzymatic machining introduces an unexplored avenue to fashion molecularly imprinted surface features via a simple process that can be accessed in virtually any laboratory. The highly-specific nature of the governing interactions lays a foundation to exquisitely control the templated nano-scale morphologies.

## ACKNOWLEDGEMENT

This work was supported by the US National Science Foundation (NSF) under grant DMR-1106005.

## REFERENCES

[1] A. Sudarsan and V.M. Ugaz, "Multivortex micromixing," *PNAS*, 8, 7228-7233(2006).

## CONTACT

Victor M. Ugaz +1-979-458-1002 or ugaz@tamu.edu